

Microcrack nucleation in granular ice under uniaxial compression: effect of grain-size and temperature

P. KALIFA, S.J. JONES AND T.D. SLADE

Institute for Marine Dynamics (NRCC), P.O. Box 12093, St. John's, Newfoundland, A1B 3T5, Canada

ABSTRACT. Uniaxial compression tests were carried out on fresh-water, isotropic, granular ice at a strain rate of $6 \times 10^{-4} \text{ s}^{-1}$. We investigated the effect of temperature (between -2 and -39°C) and grain-size (1 mm–8 mm) on the critical stress and strain at the initial crack nucleation. The amount of non-elastic strain at this event was estimated. The critical stress for initial crack nucleation increased strongly with decreasing temperature, following an Arrhenius law. It also exhibited a linear increase with $d_g^{-1/2}$ (where d_g is the average grain-size). It is shown that the results cannot be explained by the purely brittle model of Sunder and Wu (1990). The results are interpreted in terms of grain-boundary sliding, controlled by the intrinsic viscosity of the boundary.

INTRODUCTION

Microcracks are recognized as playing an important role in the deformation of polycrystalline ice over a large range of conditions. Surprisingly, the literature provides few experimental results on crack nucleation, and the physical processes for the formation of cracks are still poorly understood.

It is of general agreement that mode 1 is the main opening mode of microcracks, even under compression: this is supported by the preferential orientation of microcracks about the most compressive stress axis (Cole, 1986; Kalifa and others, 1989). The controversy resides in the physical mechanism for local stress concentration, required to break atomic bonds and create the free surfaces of the microcracks. Models for brittle materials like rocks usually assume that crack initiation is due to local tensile stress fields at the vicinity of pre-existing holes or impurities (Costin, 1985; Kemeny and Cook, 1987). Since undeformed ice does not contain such defects, other mechanisms must be considered.

At low strain rates (or low stresses), crack initiation was understood in terms of either dislocation pile-up (Gold, 1972; Cole, 1986; Schulson, 1987; Kalifa and others, 1989) or grain boundary sliding (Sinha, 1984). Although authors disagreed on the physical origin of viscoelasticity, they showed that it plays an essential role in the nucleation process. However, these mechanisms are time-dependent and may not be predominant at high strain rates. Cole (1988) calculated that dislocation pile-up is too slow to be a relevant mechanism when the amount of time for crack initiation is typically smaller than 20 s. However, he based his calculations on dislocation velocity measurements done by Fukuda and Higashi (1973) at very low

stresses (of the order of 0.1 MPa), and extrapolated linearly to higher stresses. The behaviour of dislocations at high stresses (typically 2–3 MPa) is poorly known, and this assumption has no experimental support yet. Cole (1987) and Kalifa and others (1989) observed that an increase in strain rate (typically between $5 \times 10^{-5} \text{ s}^{-1}$ and 10^{-3} s^{-1}) resulted in a change in crack location, from equally distributed at grain boundaries and within the grains, to mostly at grain boundaries.

In conditions where ice exhibits an essentially brittle behaviour, models are based on the hypothesis that the elastic anisotropy of the ice lattice is at the origin of the stress concentrations required for crack nucleation. Cole (1988) proposed a simple model by assuming that the surface energy of the crack was provided by the gradient of elastic energy between adjacent grains. This model predicts that the nucleation stress increases with decreasing grain-size. However, it does not account for the difference in nucleation stress between tension and compression, and does not address the effect of temperature on the critical stress.

Recently, Sunder and Wu (1990) used the Eshelby procedure (Eshelby, 1957) to give a detailed analysis of the internal stress fields due to the mismatch in the elastic properties of the grains. They assumed that the formation of a microcrack is controlled by the growth of a precursor (or crack nucleus) under the action of combined local and remote stress fields. They made the assumption that the precursors are generated at triple points or at grain boundary ledges, due to stress singularities. The precursor growth criterion is similar to the one of Ashby and Hallam (1986); growth occurs when the local mode 1 stress intensity factor, at the tip of the precursor, reaches a critical value K_{IC} related to the solid-vapour surface

energy of the ice. The difference in initiation stress between tension and compression is accounted for by assuming that a Coulomb friction exists between the faces of the precursor.

The present work focuses on the physical mechanisms that control the formation of microcracks in polycrystalline ice, close to the ductile–brittle transition. Uniaxial compression tests were performed on fresh-water, isotropic granular ice, at a constant strain rate of about $6 \times 10^{-4} \text{ s}^{-1}$. We investigated the effect of temperature and grain-size on the critical stress and strain for crack nucleation. Video monitoring of the tests enabled a careful investigation of crack nucleation. Direct measurements of strain on the specimens, associated with the study of both loading and unloading, allowed us to estimate the amount of anelastic strain involved in the nucleation process.

EXPERIMENTAL PROCEDURE

The specimens

Tests were performed on polycrystalline, isotropic, equiaxed ice, made at the laboratory. We used a procedure similar to the one described in Stone and others (1989). Four specimens were taken from every fabricated ice block. The grain-size of the blocks was controlled by the size of the grids used in the sieving process. Each set of sieves defined a grain-size group, within which the average specimen grain-size slightly fluctuated. The grain-size (d_g) was estimated on two thin sections at the extremities of every specimen. Between 80 and 200 grains (generally around 120) were counted on each section. d_g was calculated using the formula (Dieter, 1976)

$$d_g = (6/\pi N_A)^{1/2}, \quad (1)$$

where N_A is the number of grains per unit area.

Each specimen was manufactured on a milling machine in order to obtain cuboids of dimensions $60 \times 60 \times 120 \text{ mm}^3$. The specimens were then stored in the testing room for about 15 h to equilibrate in temperature.

Apparatus and measurements

Tests were performed with a 1 MN testing frame equipped with a servo-controlled hydraulic actuator. The end-caps were flat polished stainless steel platens. The bottom one was provided with a cooling system in order to prevent heat transfer from the oil in the actuator. The top end-cap was able to swivel in case of a small non-parallelism of the specimen extremities.

The axial load F was measured by a strain gauge load cell placed between the frame and the upper end-cap. The axial stress σ was approximated by the ratio $\sigma = F/A$, where A is the nominal cross-section area.

The axial strain was measured directly on the central part of the specimens, using LVDTs. The grips holding, respectively, the body and the core of the transducer, were fixed into the ice by a very slight melting–freezing process. The part of the grip in contact with ice consisted of a 15 mm wide and 0.5 mm thick blade, and penetrated about 1 mm into the specimen. During installation of the transducers, a plate holding the grips together ensured

parallelism and consistent spacing h . The latter was $h = 60 \text{ mm}$, each grip being 30 mm away from the closest end of the specimen. The axial strain, ϵ , was approximated to $\epsilon = d/h$, where d is the relative displacement of the grips.

Analogue outputs of the transducers were recorded on a strip chart recorder and stored as digitized data. Signals were sampled at 200 Hz during the first 15 s (including loading and unloading of the specimen) and at 20 Hz for the next 300 s.

Video monitoring

Video monitoring and recording of the specimens during the tests were done with a regular speed (30 frame s^{-1}) high resolution video camera. Microcracks were rendered visible by the reflection of a light source on their faces. Two halogen lamps facing each other were placed at 90° from the camera. Such a set-up allowed the observation of cracks with any orientation. Synchronization of the video recording was achieved by digitizing the video signal along with other outputs. Prior to the test, the camera was blinded with a black panel. The fast removal of the panel resulted in an abrupt change in the video signal; as well, it was easily determined on the video monitor as it occurred between two frames. This procedure, associated with a frame-by-frame play-back of the recording, allowed us to correlate visible events to mechanical measurements with an accuracy of $1/30 \text{ s}$.

The central event of this work is the formation of the first crack (called “crack initiation” in this paper). In order to avoid any interface effects, we considered only the cracks nucleated in the 60 mm central part of the specimen.

Testing procedure

Two series of tests were carried out at the same strain rate. In the first one, the effect of temperature was investigated on specimens with a grain-size of about 4.5 mm (group 4). Temperature was varied between -2°C and -39°C , with an accuracy of 0.5°C . In the second one, grain-size effect was studied at -10°C on six groups of specimens, covering the range 1 mm – 8 mm. Four tests were performed for each sample condition of temperature and grain-size.

In order to ensure a better ice/end-cap interface, specimens were subjected to a small pre-load (typically 0.3 MPa at -2°C , 0.7 MPa at -39°C) for 10 min, followed by a relaxation period of 30 min or more. After this period, the LVDTs no longer exhibited a change and the amount of permanent deformation was negligible.

Tests were stopped shortly after the nucleation of the first cracks (at an axial stress of 4 MPa at -10°C , 7 MPa at -39°C). Depending on the experiment, between 5 and 50 cracks were nucleated (no detailed analysis was done). At this point, the piston moved back to its initial position at a very high velocity. As a result, the load was relaxed in about 0.03 s. The elastic modulus E was then calculated according to

$$E = \sigma_m / \epsilon_m^c, \quad (2)$$

where σ_m is the maximum stress applied to the specimen and ϵ_m^c is the instantaneous relaxation strain measured by the LVDTs. Since very few microcracks were nucleated, the measured elastic modulus can be consid-

ered as the one for virgin ice. This approximation is supported by recent work which showed that a fairly high density of microcracks is necessary to alter the elastic modulus of ice (Stone and others, 1989; Kalifa and others, 1989). The elastic strain at the first crack was then merely deduced from the critical stress at this event (σ_i)

$$\epsilon_i^e = \sigma_i/E. \tag{3}$$

This calculation procedure was applied independently on both LVDTs, and on most specimens.

RESULTS AND ANALYSIS

General comments

Experimental conditions and results are summarized in Tables 1 and 2. Tests are gathered by temperature and grain-size groups. The letter in the specimen number refers to the block from which the specimen was taken. The two values given in the grain-size column correspond to the two thin sections made for each specimen. The results

involving strain measurements (that is strain rate, critical strain at the first crack, and Young's modulus) are given for both LVDTs. Also, two values appear in the columns for stress and strain: they are associated with the two video frames between which the event occurred. Note that the uncertainty is ≈ 0.15 MPa in stress, and $\approx 2 \times 10^{-5}$ in strain. This gives an inherent accuracy of better than 10% in both cases.

Although a constant strain rate was exhibited during the loading, it varied slightly from test to test. However, the LVDTs did not measure exactly the same strain rate on each side of the specimens, showing a slightly uneven deformation. The difference in measurements was generally very small. The overall average strain rate is $(6.0 \pm 0.9) \times 10^{-4} \text{ s}^{-1}$.

The duration of the loading part of the tests was of the order of 1.5 s, and the first cracks formed after about 0.7–1.0 s. The Young's modulus also exhibited small variations from test to test, as well as between transducers. The average value of Young's modulus for all tests is $E = 8.9 \pm 1.1$ GPa. This is close to the theoretical value of 9.5 GPa and demonstrates the good quality of the ice.

Table 1. Results for specimens tested at different temperatures and constant grain-size ($d_g \approx 4.5 \text{ mm}$)

Spec. no.	Temp. (°C)	Grain-size (mm)	Initiation stress (σ_i) (MPa)	LVDT No. 1				LVDT No. 2			
				Strain rate ($\times 10^{-4} \text{ s}^{-1}$)	Initiation strain (ϵ_i) ($\times 10^{-4}$)	Elastic component (ϵ_i^e) ($\times 10^{-4}$)	Elastic modulus (E) (GPa)	Strain rate ($\times 10^{-4} \text{ s}^{-1}$)	Initiation strain (ϵ_i) ($\times 10^{-4}$)	Elastic component (ϵ_i^e) ($\times 10^{-4}$)	Elastic modulus (E) (GPa)
J2	-2		1.87–2.01	4.86	2.1–2.3			6.25	2.2–2.4		
P1	-2	4.76–4.25	1.77–1.91	6.05	2.8–3.0			6.02	2.7–2.8		
T2	-2		1.44–1.55	5.25	2.4–2.6	2.3–2.5	9.10	6.16	2.9–3.1	2.3–2.5	8.91
S2	-2	4.58–4.42	1.33–1.44	3.30	1.2–1.3	1.4–1.5	9.46	6.56	1.7–2.0	1.2–1.3	9.44
H1	-10	4.14–4.02	1.83–1.97	6.32	2.4–2.6			6.48	2.5–2.7		
T1	-10	4.43–4.34	2.07–2.20	6.98	3.4–3.6	2.6–2.8	7.97	6.60	2.1–2.3	1.8–1.9	8.87
S1	-10	4.11–4.86	1.83–1.95	5.21	2.2–2.4	2.0–2.1	9.12	6.61	2.7–2.9	2.1–2.2	
J1	-10		2.18–2.32	6.51	3.0–3.1			6.69	2.8–3.0		
H3	-20	4.24–4.41	3.16–3.33	4.95	3.6–3.7			6.29	3.8–4.0		
M2	-20	4.22–4.47	2.42–2.57								
T3	-20		2.60–2.80	6.20	3.5–3.7	2.7–2.9	9.66	5.80	2.8–3.1	2.6–2.8	9.87
S3	-20		2.59–2.76	5.54	3.4–3.5	2.8–3.0	9.11	5.96	2.5–2.7	2.4–2.6	10.61
M3	-30	5.03–5.11	4.31–4.45	7.10	5.8–6.0	5.5–5.7	7.84				
J4	-30		3.74–3.90		3.6–3.8	3.6–3.8	10.26		3.4–3.5	3.4–3.5	11.01
Q1	-30	4.62–4.47	3.86–4.03	7.30	5.5–5.8			5.40	3.8–4.0		
P3	-30	4.07–4.11	4.14–4.29		4.4–4.6				3.5–3.7		
H4	-39	4.00–4.45	6.20–6.39	6.52	7.5–7.8	7.1–7.3	8.73	5.76	6.5–6.7	5.5–5.6	11.34
P4	-39	4.34–4.08	5.99–6.18	7.33	8.4–8.6	7.5–7.8	7.96				
M4	-39	5.04–4.99	6.16–6.30		8.0–8.2	6.8–7.0	9.05				
Q2	-39	4.71–4.65	5.74–5.88	5.70	5.5–5.7	5.8–5.9	9.94	4.30	4.8–5.0		

Since the non-recoverable strain at unloading was not measurable, the strain at initial crack nucleation was expressed as

$$\epsilon_i = \epsilon_i^e + \epsilon_i^c, \tag{4}$$

where the complementary component, ϵ_i^c , is essentially the delayed elastic component.

Structural observations

The frame-by-frame play-back of the video recordings is a very powerful tool for determining the time of the nucleation of the first crack and for studying the evolution of the cracks, once nucleated. Two noteworthy observations were made:

- A nucleated crack appeared first as a slightly lighter area, which kept enlarging and brightening for 2 to 4 frames. It seemed, therefore, that the crack kept growing and/or opening during this 0.07–0.14 s time period, corresponding to a stress increment of 0.3 to 0.5 MPa.

- When applied stress was released, a large proportion of cracks closed within 2 or 3 frames (0.07–0.1 s). The closure process of the remaining cracks was slower. However, less than 10% of all cracks were visible after 5 min. This phenomenon occurred in all specimens, in spite of the fact that the maximum stress was up to 1.7 times the initiation stress. Although no systematic study was done, it appeared that the first cracks to close were not necessarily the last to nucleate. Another important parameter is certainly the orientation of cracks with respect to the compression axis: axial cracks are more stable than angled cracks. This assertion was difficult to confirm on the video records, due to the size of the cracks. However, it was supported by the observation of thin sections from specimens that underwent a higher load (about 60% of the peak stress): a smaller proportion of cracks closed at unloading, and axial cracks were more open (blacker) than angled cracks.

These observations demonstrate that the application of a stress much higher than the initiation stress is required for cracks to stay open at unloading. As a result, cracks

Table 2. Results for specimens tested at $-10 \pm 0.5^\circ\text{C}$, and various grain-sizes. Results for size group number 4 are presented in Table 1

Spec. no.	Grain-size group	Grain-size (mm)	Initiation stress (σ_i) (MPa)	LVDT No. 1				LVDT No. 2			
				Strain rate ($\times 10^{-4} \text{ s}^{-1}$)	Initiation strain (ϵ_i) ($\times 10^{-4}$)	Elastic component (ϵ_i^c) ($\times 10^{-4}$)	Elastic modulus (E) (GPa)	Strain rate ($\times 10^{-4} \text{ s}^{-1}$)	Initiation strain (ϵ_i) ($\times 10^{-4}$)	Elastic component (ϵ_i^c) ($\times 10^{-4}$)	Elastic modulus (E) (GPa)
X1	1	0.82–1.18	3.11–3.27	6.61	5.0–5.2	3.8–4.0	8.09	6.37	3.5–3.7	3.7–3.8	8.52
X2	1	0.80–1.19	3.58–3.73	6.54	5.1–5.4	5.1–5.3	7.03	6.71	4.7–5.0	4.6–4.8	7.85
X3	1	0.77–1.15	3.87–4.00	6.26	5.1–5.3	5.3–5.4	7.33	6.49	5.3–5.5	4.6–4.7	8.46
X4	1	0.92–1.23	3.40–3.52	6.16	4.7–4.9	4.2–4.3	8.14	6.48	4.3–4.5	3.9–4.0	8.80
O1	2	1.36–1.49	3.91–4.04	6.14	5.0–5.1	4.7–4.8	8.33	6.74	5.9–6.1	4.9–5.0	8.06
O2	2	1.43–1.60	2.80–2.93	6.04	3.9–4.1	3.2–3.3	8.75	6.21	3.7–3.9	3.6–3.8	7.75
O3	2	1.40–1.67	3.31–3.46	6.44	4.9–5.2	4.0–4.2	8.20	5.37	4.2–4.4	4.3–4.4	7.67
V1	2	1.37–1.61	2.91–3.07	5.89	3.8–4.1	3.5–3.7	8.30	6.20	4.0–4.2	3.7–3.9	7.97
V2	2	1.36–1.53	3.74–3.89	5.82	5.0–5.2	5.1–5.3	7.38	5.76	4.7–4.9	4.3–4.4	8.78
Z1	3	2.12–2.16	2.83–2.99	6.17	4.0–4.2	3.5–3.7	8.09	6.39	3.8–4.1	3.5–3.7	8.18
Z2	3	2.21–2.46	2.89–3.00	6.61	4.4–4.6	4.0–4.1	7.28	6.10	3.4–3.6	3.1–3.2	9.34
Z3	3	2.16–2.29	2.65–2.80	6.47	3.9–4.2	3.1–3.3	8.42	6.23	3.6–3.9	3.1–3.3	8.43
Z4	3	2.10–2.21	2.94–3.00	5.92	3.7–4.0	3.5–3.7	8.31	6.72	2.7–3.0	3.7–3.8	8.01
R2	5	5.90–6.10	2.02–2.15	5.30	3.2–3.4	2.1–2.3	11.49	6.00	2.6–2.8	1.8–1.9	9.54
R4	5	5.33–5.30	2.05–2.21	6.12	2.7–3.0	2.3–2.4	9.03	5.70	2.3–2.5	2.2–2.3	9.42
U2	5	5.52–6.20	2.40–2.57	5.47	3.1–3.3	2.4–2.6	9.84	5.71	2.9–3.2	2.3–2.4	10.64
U1	5	5.52–5.67	2.05–2.21	5.78	2.4–2.6	2.3–2.5	8.79	6.83	2.9–3.1	2.3–2.5	9.04
W1	6	8.44–7.05	1.80–1.93	5.57	2.3–2.5	2.0–2.1	9.13	6.16	1.7–1.9	1.9–2.0	9.54
W2	6	9.16–6.68	2.27–2.42	4.84	2.4–2.6	2.3–2.4	9.88	6.82	3.3–3.5	2.1–2.2	10.56
W3	6	7.90–7.19	2.28–2.44	5.64	2.6–2.8	2.7–2.9	8.48	6.69	3.0–3.3	2.7–2.9	8.30
W4	6	8.46–6.79	2.67–2.85	6.51	3.2–3.5	3.0–3.2	8.91	7.07	4.3–4.6	3.0–3.2	8.66

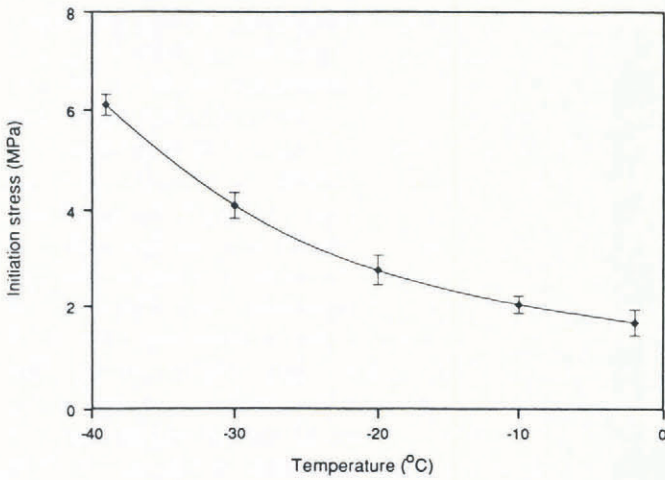


Fig. 1. Initiation stress versus temperature, for a grain of about 4.5 mm (size group number 4). The points and the error bars are, respectively, the average and the standard deviation of the 4 tests carried out at every temperature.

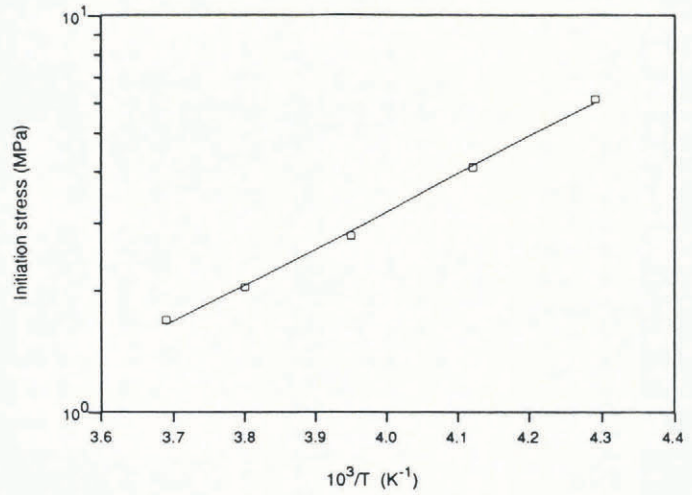


Fig. 2. Initiation stress versus the inverse of temperature on a linear-log scale. Each data point represents the average of 4 tests, and the line is a linear regression through the points.

may not act as an efficient factor to modify the local stress fields, and, hence, the bulk mechanical properties of the specimen, until the stress reaches this level. This stage is probably reached close to the peak (or failure) stress. This behaviour is consistent with observations made by Cole (1990). At a strain rate of 10⁻³ s⁻¹, he observed that the stress for failure was significantly higher than the one corresponding to the end of cracking activity.

Temperature effect

On Figures 1 and 3, the data points represent the average of the four tests carried out at each temperature. The error bars correspond to the standard deviation across the four tests, and include the error inherent in the method of observation.

On Figure 1 the initiation stress, σ_i , is plotted as a function of temperature. Tests exhibited a very good repeatability: the standard deviation varied between 0.18 and 0.31 MPa. The striking feature of this figure is the very important increase in the initiation stress with decreasing temperature. On average, σ_i increases from 1.67 MPa at -2°C to 6.10 MPa at -39°C. Unfortunately, the effect of temperature has not been investigated previously in this strain-rate range in uniaxial tension. The only previous investigation was performed at a strain rate of 10⁻⁶ s⁻¹, more than two orders of magnitude smaller than that studied here (Schulson and others, 1984). Schulson and others observed that for a grain-size of 4.5 mm, $\sigma_i \approx 1.2$ MPa and did not change with temperature between -5°C and -20°C.

The temperature dependence of σ_i can be described with an Arrhenius law

$$\sigma = \sigma_0 \exp(Q/RT), \tag{5}$$

where T is the absolute temperature, R is the gas constant and σ_0 is a constant. On Figure 2, $\log(\sigma)$ is plotted as a function of $1/T$. The slope of the linear regression through the data points gives an apparent activation energy $Q \approx 19$ kJ mol⁻¹.

On Figure 3, the initiation strain ϵ_i is plotted versus temperature. Although strain data present more scatter than stress data, they exhibit essentially the same temperature dependence. On average, ϵ_i increases from 2.3×10^{-4} at -2°C to 6.8×10^{-4} at -39°C. The linear elastic component, ϵ_i^c , is reported in Tables 1 and 2; it forms the major part of the total strain (between 75% and 95%), whereas the complementary component, ϵ_i^p , reaches an average level of the order of 5×10^{-5} (Table 3). However, there are large standard deviations associated with ϵ_i^c , both from test to test and between LVDTs. A small inaccuracy in the Young's modulus measurement, due to either uneven loading or the method of strain measurement, leads to a large inaccuracy in ϵ_i^c . Thus, it is not surprising that ϵ_i^c exhibits a large scatter between LVDTs. No temperature effect on ϵ_i^c is observed.

Grain-size effect

The initiation stress, σ_i , is plotted versus $d_g^{-1/2}$ in Figure 4.

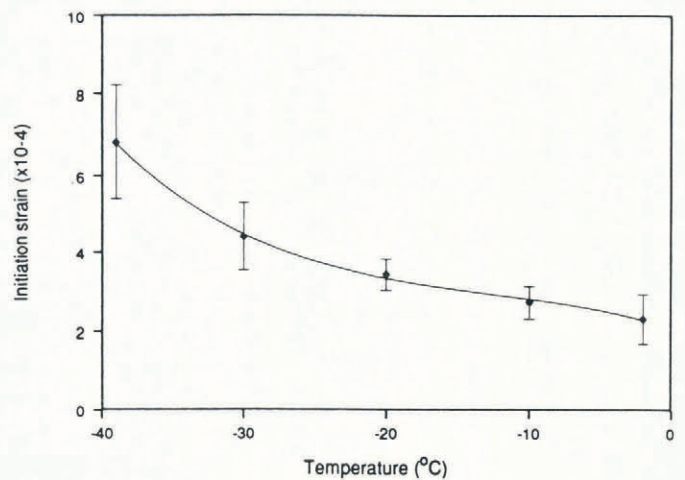


Fig. 3. Initiation strain versus temperature for a grain of about 4.5 mm (size group number 4). The points and the error bars are, respectively, the average and the standard deviation of the 4 tests carried out at every temperature.

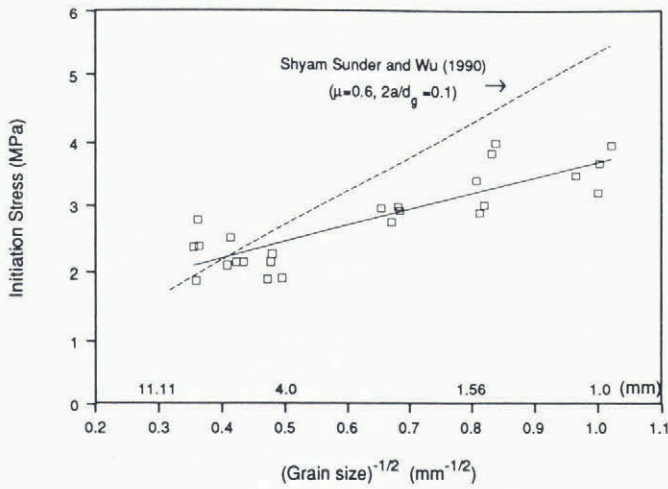


Fig. 4. Initiation stress versus grain size, at $T = -10^{\circ}\text{C}$. Also drawn is a linear regression through the data points and a theoretical curve derived from the model of Sunder and Wu (1990).

Table 3. Estimated non-elastic (or complementary) strain at the first crack, ϵ_1^c , as a function of temperature.

Temp. ($^{\circ}\text{C}$)	-2	-10	-20	-30	-39
Compl. strain ($\times 10^{-5}$)	3 ± 3	5 ± 3	4 ± 3	2 ± 2	7 ± 5

The coordinates of each data point are the average of the two values given in Table 2, for σ_1 and d_g , respectively. Superimposed is a linear regression through the data points (solid line), as well as a theoretical curve which will be discussed later. In spite of the scatter in the data points, the initiation stress exhibits a linear increase with $d_g^{-1/2}$; on average, σ_1 decreases from 3.7 to 2 MPa as d_g increases from 1 mm to 8 mm.

These values are similar to the value of 2.5 MPa obtained by Kalifa and others (1989) under the same conditions. However, they are significantly smaller than the critical stress of 3.5 MPa obtained by Cole (1990) at 10^{-3} s^{-1} on the same type of ice. The same trends are observed for the grain-size dependency of the initiation strain. Again, the major part of the strain is linear elastic (between 79 and 91% of ϵ_1), and ϵ_1^c reaches an average value of the order of 5×10^{-5} (Table 4). The large

Table 4. Estimated non-elastic (or complementary) strain at the first crack, ϵ_1^c , as a function of grain-size. Result for size group number 4 appears in Table 3.

Size group	1	2	3	5	6
Compl. strain ($\times 10^{-5}$)	4 ± 4	4 ± 4	4 ± 2	6 ± 3	4 ± 5

standard deviations do not allow us to distinguish any grain-size effect on ϵ_1^c .

DISCUSSION

The most striking result of our experiments is the very strong increase in the initiation stress with decreasing temperature. Temperature may affect the nucleation criterion and/or the physical mechanism necessary to achieve it. The nucleation criterion can be expressed as the fracture toughness, K_{1C} , related to the vapour-solid surface energy of the ice (Lawn and Wilshaw, 1975). Surface energy measurements seem to show that it is independent of temperature (Hobbs, 1974). This is supported by uniaxial tension tests at 10^{-6} s^{-1} , mentioned previously (Schulson and others, 1984), which showed that temperature had no effect on σ_1 between -5 and -20°C . Therefore, the temperature dependency of the initiation stress would seem to be due to the physical mechanism necessary to reach the criterion.

Following Sunder and Wu (1990), the effect of temperature on σ_1 is addressed by introducing Coulomb friction between the faces of the precursor. The only investigation in ice-ice friction available in the literature was performed recently by Jones (1989) and partly reported by Schulson (1990). It was shown that the temperature dependency of the dynamic friction coefficient, μ , was a function of sliding velocity. In our experiments, it is difficult to determine the relationship between the bulk strain rate and the sliding velocity (V) of the precursor faces. In a first step, we assume that $V = \dot{\epsilon} \times 2a$, where $2a$ is the length of the precursor. Taking $2a/d_g = 0.1$ (Sunder and Wu, 1990), with $\dot{\epsilon} = 6 \times 10^{-4} \text{ s}^{-1}$ and $d_g = 4.5 \text{ mm}$, we obtain $V = 2.7 \times 10^{-7} \text{ m s}^{-1}$. This value is probably a lower bound and the actual velocity may be much higher. In this range, Jones (1989) showed that μ is essentially independent of temperature. Furthermore, he estimated that the largest variation in μ , achieved at a velocity of 10^{-4} m s^{-1} , was only between 0.25 and 0.77 when the temperature decreased from -3°C to -40°C . On the other hand, Sunder and Wu predicted that, for $2a/d_g = 0.1$ and $d_g = 4.5 \text{ mm}$, an increase in σ_1 from 2 MPa to 3 MPa required a variation in the coefficient of friction between the faces of the precursor from 0.2 to 1.0. One may argue that the physical conditions in the friction tests are not the same as in our crack nucleation tests: for example, different sizes of the surfaces in contact, surfaces exposed to atmosphere as opposed to vacuum or water vapour. Despite these differences, it is clear that the strong temperature dependency of the initiation stress (between 1.67 MPa at -2°C and 6.1 MPa at -39°C) would require a much larger change in friction coefficient than has been observed. Another discrepancy appears on Figure 4, showing the effect of grain-size on σ_1 : the slope of the theoretical curve derived from Sunder and Wu, for $\mu = 0.6$ and $2a/d_g = 0.1$, is larger than that obtained from the linear regression through the data points.

Therefore, in the conditions studied, it is clear that crack nucleation is not controlled by the growth of a precursor. However, the generation of the precursor itself may be the controlling mechanism. It would then be more suitable to call it a "crack nucleus". It is probable that when the local criterion for the formation of the crack

nucleus is achieved, the latter grows catastrophically into a microcrack of visible size, using the energy available in the neighbouring grains.

The physical mechanisms at the origin of the stress concentration for the formation of the crack nucleus are now to be addressed. The level of the complementary strain seems too low for trans-granular dislocation pile-up to be considered as an efficient stress concentrator. However, as pointed out by Raj and Ashby (1971), a very small grain boundary sliding (corresponding, for polycrystalline ice, to a delayed elastic strain typically less than 10^{-4}) is required to build up stresses at grain boundary ledges or triple points. It is clear that the elastic anisotropy of the ice lattice generates high stresses on the grain boundaries, which enable them to slide. However, this sliding is controlled by the mechanical properties of the boundaries themselves. The latter may be characterized by a viscosity or an internal friction, which would increase with decreasing temperature. Such an hypothesis needs to be supported by more experiments concerning, in particular, the structure of the grain boundaries. However, it seems to be a reasonable explanation for the large increase in the nucleation stress with decreasing temperature. Consistent with this, the initiation stress in uniaxial tension should also increase with decreasing temperature.

At temperatures above -10°C , pressure melting may occur at the grain boundary ledges or triple points (Hobbs, 1974), and must be considered as a possible stress relieving mechanism.

CONCLUSIONS

Uniaxial compression tests were carried out on isotropic granular ice, at a strain rate of about $6 \times 10^{-4} \text{ s}^{-1}$. We investigated the effect of temperature and grain-size on the critical stress and strain at the formation of the first crack and estimated the elastic and non-elastic components of strain at this event. Video monitoring of the specimens during the tests allowed us to study the behaviour of the microcracks during both loading and unloading. It appeared that many microcracks closed soon after unloading, although the maximum stress undergone by the specimens was up to 1.7 times the initiation stress.

The initiation stress exhibited a strong increase with decreasing temperature. Furthermore, the initiation stress appeared to increase linearly with $d_g^{1/2}$, where d_g is the average grain-size of the specimens. Moreover, it was shown that the major part of the initiation strain was linear elastic, and that the delayed elastic component reached about 5×10^{-5} , with a large scatter.

It was demonstrated that these results cannot be explained by a purely brittle model based only on the elastic anisotropy of the ice lattice, and that non-elastic mechanisms must be considered. It is proposed that, in the conditions studied, crack nucleation is controlled by the formation of a crack nucleus, which grows into a visible microcrack. The formation of the crack nucleus at triple points or grain boundary ledges is probably driven by the high local stresses due to the elastic anisotropy of the ice lattice. However, it may be controlled by the internal friction of the grain boundaries themselves.

ACKNOWLEDGEMENTS

We thank B.L. Parsons and F.M. Williams for helpful comments.

REFERENCES

- Ashby, M.F. and S.D. Hallam. 1986. The failure of brittle solids containing small cracks under compressive stress states. *Acta Metall.*, **34**, 497-510.
- Cole, D.M. 1986. Effect of grain size on the internal fracturing of polycrystalline ice. *CRREL Rep.* 86-5.
- Cole, D.M. 1987. Strain-rate and grain-size effects in ice. *J. Glaciol.*, **33**(115), 274-280.
- Cole, D.M. 1988. Crack nucleation in polycrystalline ice. *Cold Reg. Sci. Technol.*, **15**(1), 79-87.
- Cole, D.M. In press. Microfracturing and the compressive failure of polycrystalline ice. In Jones, S.J., R. McKenna, J. Tillotson, and I.J. Jordaan, eds. *IUTAM/IAHR Symposium on the Ice/Structure Interaction, St. John's, Newfoundland, Canada, August 14-17, 1989*. Berlin, etc. Springer-Verlag.
- Costin, L.S. 1985. Damage mechanics in the post-failure regime. *Mech. Materials*, **4**, 149-160.
- Dieter, G.E. 1976. *Mechanical metallurgy*. New York, McGraw-Hill.
- Eshelby, J.D. 1957. The determination of the elastic field of an ellipsoidal inclusion, and related problems. *Proc. R. Soc. London, Ser. A*, **241**, 376-396.
- Fukuda, A. and A. Higashi. 1973. Dynamical behavior of dislocation in ice crystals. *Cryst. Lattice Defects*, **4**(3), 203-210.
- Gold, L.W. 1972. *The process of failure in columnar-grained ice*. Ottawa, National Research Council of Canada. Division of Building Research. (Research Paper 523.)
- Hobbs, P.V. 1974. *Ice physics*. Oxford, Clarendon Press.
- Hondoh, T. and A. Higashi. 1983. Generation and absorption of dislocations at large-angle grain boundaries in deformed ice crystals. *J. Phys. Chem.*, **87**(21), 4044-4050.
- Jones, D.E. Unpublished. An experimental investigation of low-speed ice-ice friction. (Masters thesis, Dartmouth College. Thayer School of Engineering. 1989.)
- Kalifa, P., P. Duval, and M. Ricard. 1989. Crack nucleation in polycrystalline ice under compressive stress states. In Sinha, N.K., D.S. Sodhi, and J.S. Chung, eds. *Proceedings of the Eighth International Conference on Offshore Mechanics and Arctic Engineering 1989, The Hague, the Netherlands, March 19-23, 1989. Vol. 4. Arctic and polar technology*. New York, American Society of Mechanical Engineers, 13-21.
- Kemeny, J.M. and N.G.W. Cook. 1987. Crack models for the failure of rocks in compression. *Proceedings of the 2nd International Conference on Constitutive Laws for Engineering Materials, Tucson, AZ*.
- Lawn, B.R. and T.R. Wilshaw. 1975. *Fracture of brittle solids*. Cambridge, Cambridge University Press.
- Raj, R. and M.F. Ashby. 1971. On grain boundary sliding and diffusional creep. *Metal Transactions*, **2**, 1113-1127.
- Schulson, E.M. 1987. The fracture of ice Ih. *J. Phys. (Paris)*, **48**, Colloq. C1, 207-220. (Supplément au 3.)
- Schulson, E.M. In press. The brittle compressive fracture of ice. *Acta Metall.*

- Schulson, E.M., P.N. Lim, and R.W. Lee. 1984. A brittle to ductile transition in ice under tension. *Philos. Mag.*, **49**(3), 353-363.
- Sinha, N.K. 1984. Intercrystalline cracking, grain-boundary sliding, and delayed elasticity at high temperatures. *J. Mater. Sci.*, **19**(2), 359-376.
- Stone, M., I.J. Jordaan, S.J. Jones, and R.M. McKenna. 1989. Damage of isotropic polycrystalline ice under moderate confining pressures. In Axelsson, K.B.E. and L.Å. Fransson, eds. *POAC 89. The 10th International*

- Conference on Port and Ocean Engineering under Arctic Conditions, June 12-16, 1989, Luleå, Sweden. Proceedings. Vol. 1.* Luleå, Tekniska Högskolan i Luleå, 408-419.
- Sunder, S.S. and M.S. Wu. 1990. Crack nucleation due to elastic anisotropy in polycrystalline ice. *Cold Reg. Sci. Technol.*, **18**(1), 29-47.

The accuracy of references in the text and in this list is the responsibility of the authors, to whom queries should be addressed.